A Transparent Antipeep Piezoelectric Nanogenerator to Harvest Tapping Energy on Screen

Caixia Hu, Li Cheng, Zhe Wang, Youbin Zheng, Suo Bai, and Yong Qin*

With the fast development of electronics, various portable personal electronic products, such as cell phones and tablets with touch screens, are being extensively used across the world. We frequently tap the screens to communicate with each other, control some instruments, or achieve some other goals. In these conditions, much mechanical energy is generated during the tapping process. If this mechanical energy could be collected and converted into electricity to charge the battery, the working time of these portable devices could be extended significantly. As a kind of device converting mechanical energy into electrical energy, nanogenerators[1–13] (NGs) have the potential to be utilized for harvesting the tapping energy. Triboelectric NGs have been developed to harvest the tapping energy in portable electronics.[14–16] However, most touch screens are capacitive, so NGs harvesting tapping energy must be transparent and shouldn't shield the electric field. As a result, it is quite crucial to search for a new kind of flexible and transparent nanogenerator (FTNG) to harvest the tapping energy on capacitive screens.

Compared with triboelectric NGs, piezoelectric NGs have better environmental adaptability and stronger robustness. It is however challenging to develop a FTNG with high performance. In practice, an effective way to fabricate a flexible NG with high output has been achieved by mixing inorganic piezoelectric nanomaterial and polymer.[17–19] However, these kinds of NGs are nontransparent and unsuitable to harvest the tapping energy on screen. Fortunately, the alignment of the filler in the composite is one of the factors enhancing its transparency and piezoelectric coefficient. For example, the light transmittance of aligned carbon nanocoils dispersed in isopropyl alcohol is two to three times higher than that of randomly oriented nanocoils.[20] Oriented $PbZr_{0.52}Ti_{0.48}O_3$ (PZT) nanowires/polyvinylidene fluoride (PVDF) composite film can lead to a larger energy density of 51.6% than that of a sample with no oriented alignment.[21] Therefore, aligning

the piezoelectric materials in a polymer-based composite NG may be an effective way to enhance its light transparency and output energy. In previous works, many methods,[22] such as the template-assisted method,[23] electrostatic spinning,[24] hydrothermal,[25] dielectrophoresis,[20,26–28] uniaxial strain,[21] liquid crystal-assisted orientation,[29] and surface-patterning techniques,[30] have been used to align these piezoelectric materials. Among these methods, dielectrophoresis is a relatively simpler and more convenient one. So in this work, we prepared the well-aligned PZT nanowires (NWs)/polydimethylsiloxane (PDMS) composite film (ANWF) by dielectrophoresis. The light transmittance of high concentration composite film was increased from 42% of the random aligned PZT NWs/PDMS composite film (RNWF) to 72% of ANWF. Based on these films, we fabricated NGs with a thick Kapton film substrate. The output voltage 0.60 V and current 3.95 nA of ANWF NG are 88% and 62% larger than those of RNWF NG, respectively. Furthermore, we fabricated a FTNG based on low concentration ANWF, which could be used for collecting the tapping energy on the touch screen of a cell phone. When the screen was lightly tapped, the output current of FTNG reached 0.8 nA. At the same time, the FTNG showed good antipeep properties when it was pasted onto a screen.

To prepare the ANWF, PZT nanofibers synthesized by electrospinning[31] were first ground into NWs in an agate mortar. As is shown in the scanning electron microscope (SEM) image of **Figure 1**a, the length and diameter of PZT NWs were about 4 μm and 700 nm, respectively. The X-ray diffraction spectrum (the insert of Figure 1a) demonstrates that the NWs are polycrystalline PZT with a perovskite structure. The PZT NWs, dimethyl siloxane, and curing agent were mixed at the mass ratio of 1:10:1, and then filled in the 150 μm gap between two pieces of indium tin oxide (ITO) glass with their conducting layer facing each other. After the bubbles in the mixture were removed under vacuum, the two pieces of ITO glass were connected to an alternating current (AC) power (50 Hz) to supply an electrical field of 1.47 V μm⁻¹, and then placed at 25 °C for 24 h to cure the mixture (Schematized in Figure 1b). In this process, PZT NWs were aligned in the electric field. The ANWF was fabricated after the ITO glass was removed. The RNWF was fabricated under the same process with ANWF except for the connection to the AC power for aligning the NWs.

To clearly observe the alignment of PZT NWs in the films under SEM, the slices of RNWF and ANWF were treated by reactive ion etching (RIE)[32–34] to have the PDMS etched

C. Hu, Dr. L. Cheng, Z. Wang, Dr. Y. Zheng,
Dr. S. Bai, Prof. Y. Qin
Institute of Nanoscience and Nanotechnology
Lanzhou University
Lanzhou 730000, China
E-mail: qinyong@lzu.edu.cn
Dr. S. Bai, Prof. Y. Qin
The Research Institute of Biomedical Nanotechnology
Lanzhou University
Lanzhou 730000, China
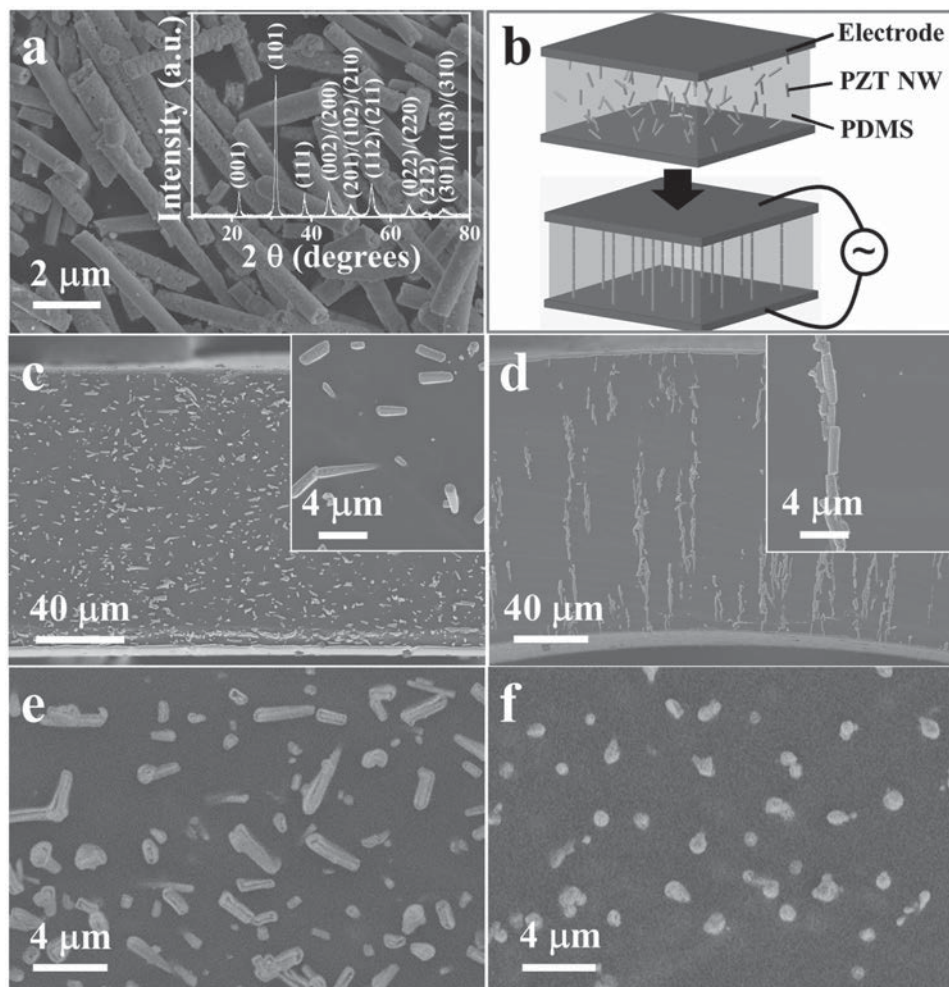
Figure 1. Fabrication of ANWF and RNWF: a) SEM image of the PZT NWs. The inset is PZT NWs' X-ray diffraction spectrum. b) Schematic image of the PZT NWs' orientation process. c,d) Crosssectional-view SEM images of RNWF and ANWF after RIE treatment, respectively. The insets are their high magnification SEM images. e,f) Top-view SEM images of RNWF and ANWF after RIE treatment, respectively.

and the PZT NWs exposed on the surface of the slices. The cross-sectional SEM images of RNWF and ANWF are shown in Figure 1c,d, respectively. The view direction is perpendicular to the direction of the electric field. We can see that NWs in the RNWF are randomly aligned, while NWs in the ANWF are aligned well along the direction of the electric field to form chains. Furthermore, the top view SEM images of RNWF and ANWF are shown in Figure 1e,f, respectively. Only the end of PZT NWs in ANWF can be observed when they were viewed along the direction of the electric field. That is, the NWs in ANWF are aligned along the view direction. As for the RNWF, both ends and sides of the PZT NWs can be observed, further confirming that the NWs were randomly aligned.

The process, during which PZT NWs aligned along the direction of electric field and then formed chains, can be explained by the principle of dielectrophoresis. First, two ends of PZT NWs will induct opposite charge in the electric field between parallel-plate electrodes. So the NWs have a torque along the electric field direction under the electric field force (**Figure 2**a).[35] Thereby, the NWs will turn along the electric field direction. Meanwhile, PZT NWs can attract each other

along their length direction because of the opposite charges (Figure 2b). So, PZT NWs form chains along the electric field direction.[26] And the chains will repel each other because of charges' repulsive force (Figure 2c). Finally, the chains stay repelled at an equal distance to reach an equilibrium state (Figure 2d).[36]

The process of aligning PZT NWs can be influenced by electric field intensity and curing temperature (*T*). When the electric field intensity increases, the force acting on NWs will increase. Thus, the NWs will turn along the electrical field faster, that is, the time needed to orient the NWs will be shorter. The light transmittance of film will be increased because the scattering of visible light will be reduced after the NWs were oriented. The visual result of NWs oriented in different electric field intensities at different times was shown in Figure S1 (Supporting Information). Two devices, which were made of two pieces of ITO glass with the mixture between them, were placed on a piece of paper with "nano" marks. The mixture under 1.47 V µm⁻¹ electric field needed 2 min to reach an equilibrium state, while the other under 0.37 V µm⁻¹ electric field needed 3 h. This confirmed that the time for orienting the NWs in 0.37 V µm⁻¹ electric
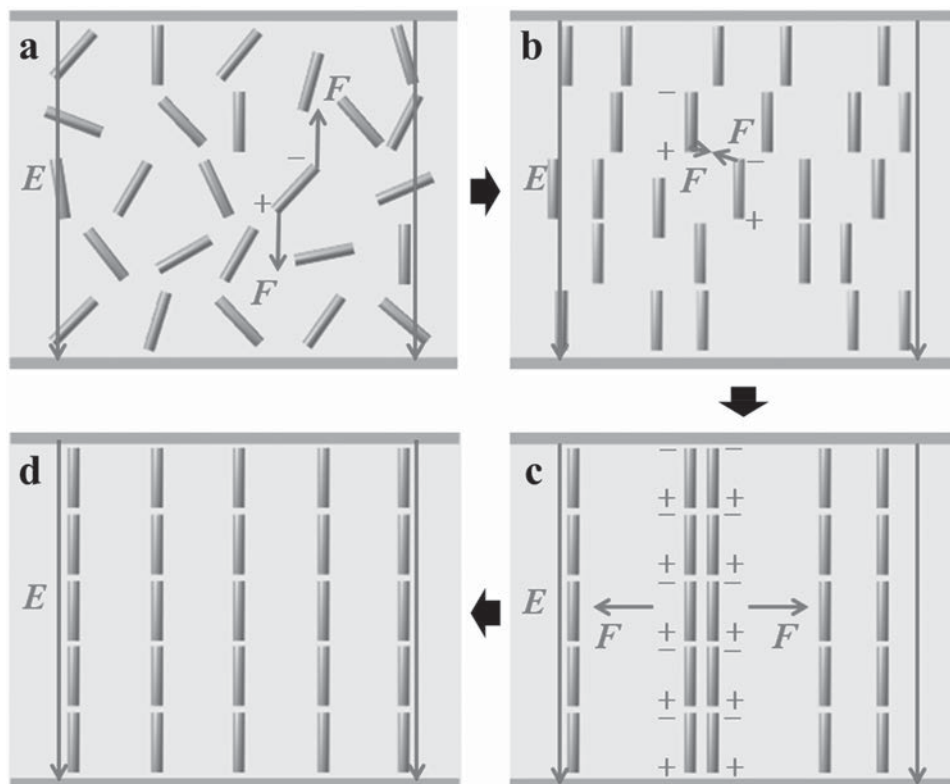
Figure 2. Schematic image of PZT NWs' orientation process in the electric field: a) Two ends of PZT NWs induct opposite charge in the electric field and NWs will turn along the electric field direction. b) NWs attract each other because of the opposite charges, and the NWs form chains along the electric field direction. c) The chains repel each other because of the repulsive forces of the charges. d) The chains will stay with an equal distance to reach an equilibrium state.

field is longer than that at 1.47 V μm^{-1} when they were cured at 25 °C. The influence of temperature on the PZT NWs orientation was shown in Figure S2 (Supporting Information). The chains formed with NWs at 100 °C were not well aligned along the electric field direction, while the NWs were aligned well at 25 °C. This can be explained as that PDMS will expand when it is cured at a high temperature.

A previous study has shown that the piezoelectric properties of piezoelectric particle-polymer matrix composites can be enhanced by aligning the particles.[37] So the ANWF was expected to possess higher piezoelectric performance than RNWF. To verify this hypothesis, NGs based on ANWF and RNWF were fabricated (see the Experimental Section). Their schematic is shown in **Figure 3**a. The NGs were polarized at 130 °C by applying a voltage of 1000 V for 1 h beforehand. Their performance was measured by stretching (2 N stretching force) the NGs in constant amplitude and frequency (0.357 Hz) driven by a linear motor. As shown in Figure 3b, the open-circuit voltages of NGs made up of RNWF and ANWF are 0.32 and 0.60 V, respectively. And the short-circuit currents of NGs made up of RNWF and ANWF are 2.44 and 3.95 nA, respectively (Figure 3c). Compared with those of the NG made up of RNWF, the output voltage and current of NG made up of ANWF are increased by 88% and 62%, respectively, which indicates that the piezoelectric performance of ANWF is better than that of RNWF. To study its frequency response ability, the NG based on ANWF is tested under different frequencies. Under a fixed stretching force at

2 N, the linear motor is adjusted to provide a series of frequency, from 0.071 to 0.357 Hz with a step of 0.071 Hz. The open-circuit voltage and short-circuit current of the NG are depicted in Figure 3d,e, respectively. This result demonstrated that the NG had the ability to harvest energy at different frequencies.

The light transmittance of the films was measured subsequently. Two mixtures were made beforehand. Mixture A is the PDMS composite mixed with high concentration PZT NWs (PZT NWs, dimethyl siloxane and curing agent at the mass ratio of 1:10:1), while mixture B is the PDMS composite mixed with low concentration PZT NWs (the above mass ratio of 1:20:1). Then four samples were prepared. Sample A and Sample B are the high concentration RNWF and ANWF, respectively, which are made up of mixture A. Sample C and Sample D are the low concentration RNWF and ANWF, respectively, which are made up of mixture B. The light transmittance of sample A, sample B, sample C, and sample D is about 42%, 72%, 60%, and 85%, respectively (**Figure 4**a). It can be concluded that both orienting the PZT NWs and decreasing the concentration of PZT NWs can reduce the scattering of visible light and thus improve the light transmittance of the films. The different light transmittance of the four samples can be observed more intuitively from Figure 4b. The four samples were placed on a piece of paper with "E" marks. We can see that the pattern character under sample D looks the clearest, followed by sample B, sample C, and sample A in that order. The larger the light
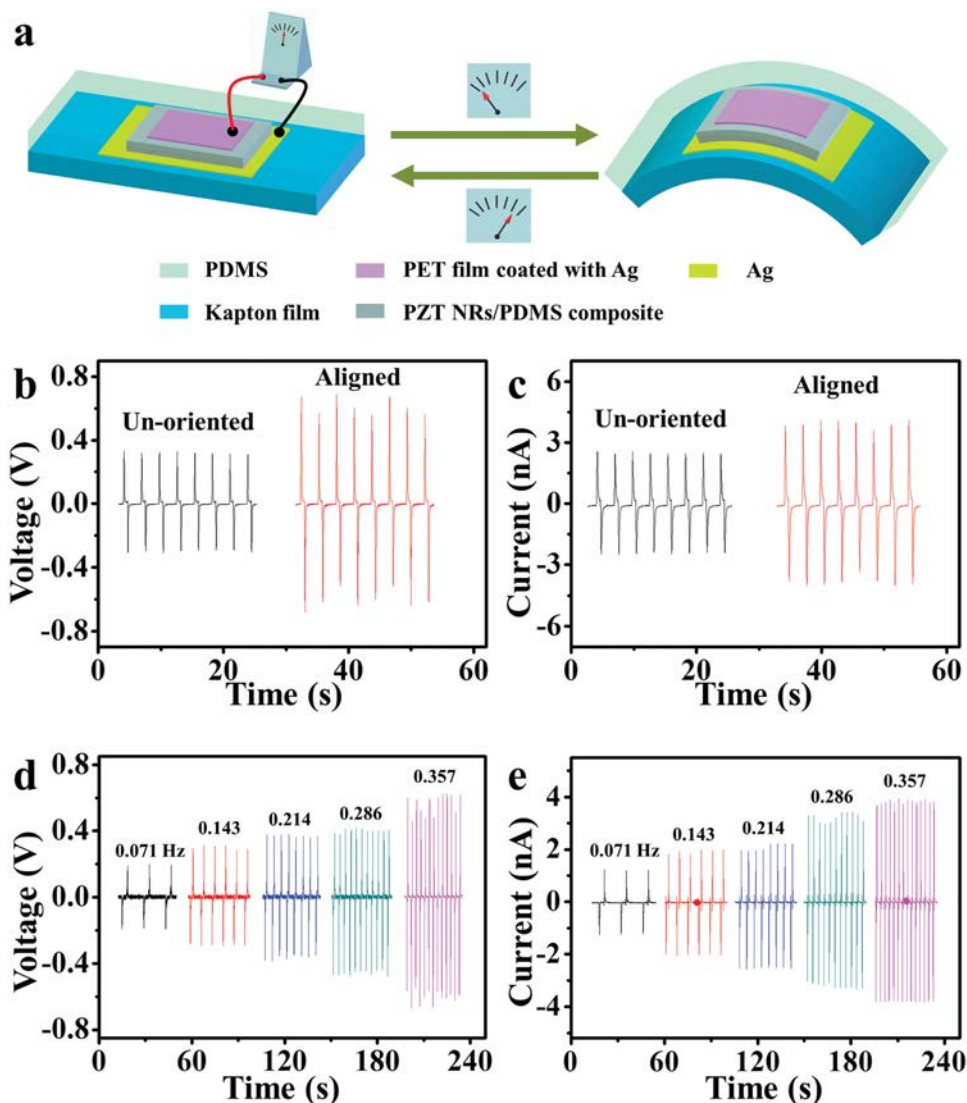
Figure 3. Measurement of NG based on ANWF and RNWF at 2 N stretching force: a) Schematic images of the NG's structure and working process. b) Open-circuit voltage and c) short-circuit current of NGs with RNWF (Un-oriented) and ANWF (Oriented) at a frequency of 0.357 Hz. d) Open-circuit voltage and e) short-circuit current of the NG based on ANWF under different frequency.

transmittance, the clearer the pattern character under the films. In order to choose a suitable thickness of low concentration ANWF, their light transmittance and the output of the FTNGs based on them are measured (Supporting Information, Figure S3). The light transmittance decreases and the output increases with increasing thickness. Taking these two factors into consideration, we choose an ANWF with 150 μm thickness in order to obtain a relatively larger light transmittance and output. As mentioned before, the NWs in ANWF formed chains array, which had an anisotropic structure for light propagation. The angle between normal direction of film and view direction is defined as θ. The transmissivity (I_e/I_i), i.e. the ratio of the emergent light (I_e) and incident light (I_i) at different angles of θ, was detected by the photoluminescence detector. When θ is 0°, 20°, and 40°, the transmissivity of ANWF with 4.35 wt% PZT NWs is about 95%, 75%, and 20%, respectively (Figure 4c). In order to show the property of antipeep intuitively, the ANWF was put on a piece of paper printed with the word "nanogenerator." The word

"nanogenerator" became blurred gradually with the increase of viewing angle. These results indicate that the ANWF has good antipeep property.

Because of the ANWF's flexibility, excellent light transmittance, piezoelectric property and good antipeep property, it is expected to be used in harvesting the tapping energy on touch screen. So we further fabricated a FTNG with interdigital pattern as shown in the schematic **Figure 5**a based on the low concentration ANWF (the detailed fabrication process is given in the Experimental Section). After being fabricated, the FTNG was polarized at 130 °C under a voltage of 1000 V for 1 h beforehand and then pasted on a cell phone's screen. We can see the pattern in the screen looked clear when θ is 0°, and it became blurred as θ increased from 0° to 40°. It showed that the FTNG had good transparency, good antipeep property and no color difference on the touch screen (Figure 5b). Then FTNG was lightly tapped (see the video and Figure 5c), which made it output a short-circuit current of 0.8 nA (Figure 5d) and an open-circuit voltage of 60 mV
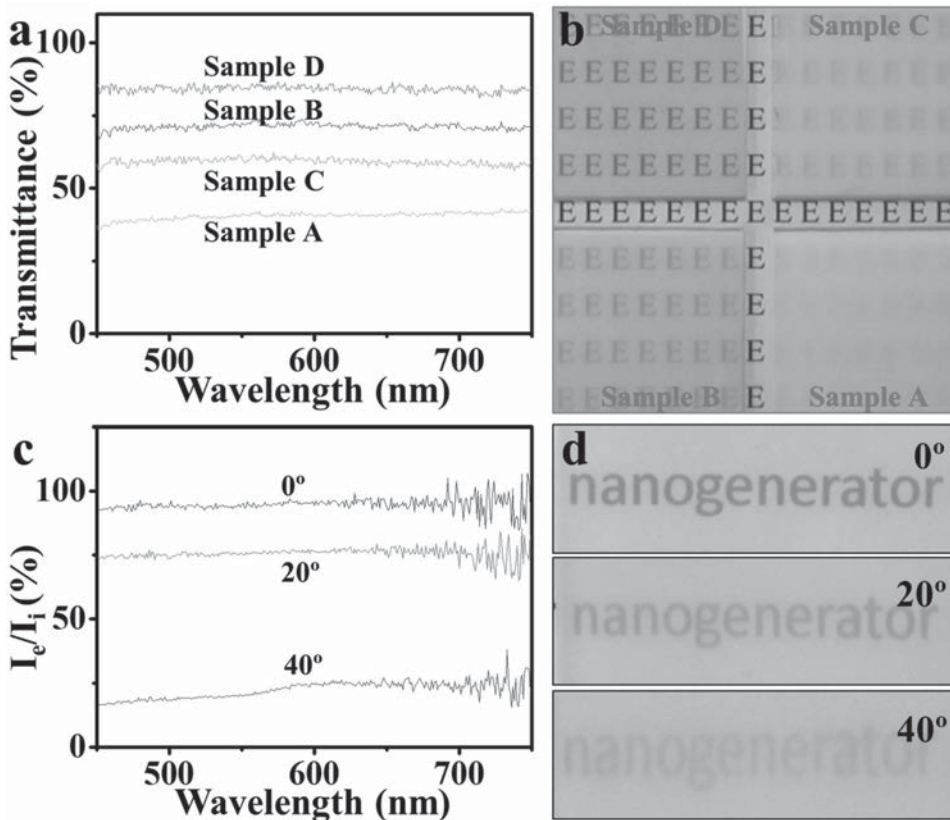
Figure 4. Optical property of ANWF: a) The light transmittance of ANWFs and RNWFs with different concentrations of PZT NWs. b) Optical images of ANWFs and RNWFs with different concentrations of PZT NWs put on a piece of paper with "E" marks. c) The transmissivity (I_e/I_i) of low concentration ANWF when θ is 0°, 20°, and 40°. d) Optical images of low concentration ANWF put on a piece of paper with "nanogenerator" mark viewing at 0°, 20°, and 40°.
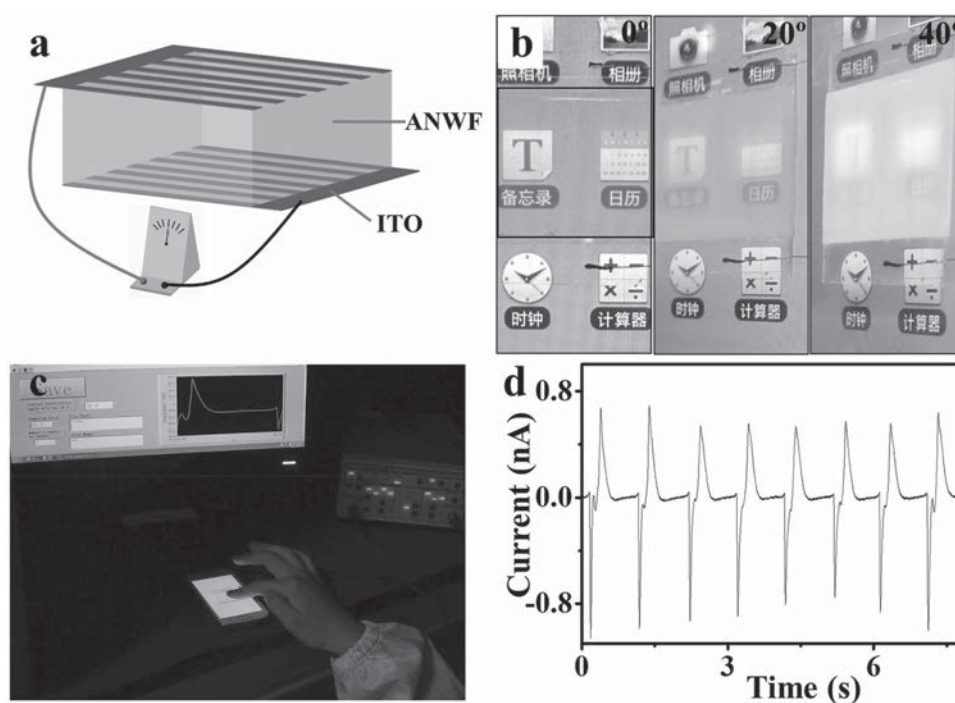
Figure 5. FTNG and its application on touch screen: a) Schematic image of the structure of FTNG. b) Optical images of FTNG pasted on cell phone when θ is 0°, 20°, and 40°. c) Photograph shows that FTNG harvests the tapping energy on cell phone screen. d) Short-circuit current of FTNG pasted on cell phone screen driven by finger tapping.

(Supporting Information, Figure S4). During the whole process, the cell phone worked well and was not influenced by FTNG, illustrating that the FTNG can successfully harvest tapping energy on a touch screen. And the output of sliding mode is seen in Figure S5 (Supporting Information). In order to test its reliability, the output of FTNG was measured each 24 h for 3 days after being polarized. (Supporting Information, Figure S6) It can also harvest the tapping energy 3 days later.

In summary, we prepared ANWF by dielectrophoresis. The PZT NWs in ANWF were well aligned along the direction of electric field. The output voltage and current of ANWF NG were obviously larger compared with those of RNWF NG, which indicates that ANWF's piezoelectric performance is much higher than RNWF's. Moreover, ANWF has better light transmittance than RNWF and it can be used as anti-peep film because of the well aligned PZT NWs in ANWF. We further fabricated FTNG based on ANWF and successfully harvested the tapping energy on screen. The output current of 0.8 nA was obtained and the cell phone worked well without being influenced by FTNG. Additionally, the FTNG played an important role in protecting privacy.

Experimental Section

RIE Treatment of ANWF and RNWF: The ANWF and RNWF were placed into the chamber, then evacuated to a base pressure of 1×10^{-4} Pa. O_2 and CF_4 were introduced at a flow rate of 54 and 14 sccm, respectively, and the glow discharge was ignited at 100 W in a working pressure of 0.6 Pa for 50 min.

Fabrication of NGs Based on ANWF and RNWF: Ag was sputtered on Kapton film substrate (3.0 cm × 3.5 cm) with 250 μm thickness as an electrode. Then the ANWF (1.0 cm × 1.2 cm × 0.015 cm) or RNWF (1.0 cm × 1.2 cm × 0.015 cm) was stuck on the substrate. Subsequently, double side silver-plated PET film (0.8 cm × 1.0 cm) with 100 μm thickness was pasted on high concentration ANWF or RNWF served as the top electrode. Cu wires were attached to the electrodes by carbon paste. Finally, a package layer of PDMS covered the device and the NG was fabricated completely.

Characterization: The light transmittance was obtained using TU1901 spectrometer by $BaSO_4$ as a reference. The light detector of Fluorlog-3 spectrofluorometer equipped with 450 W xenon lamps (Horiba Jobin Yvon) is used to measure the light intensity at different angles of θ. A LED flat lamp acts as a light source. And then the film is placed on the surface of the LED. The light intensity at a different angle θ is measured again.

Fabrication of FTNG: Two pieces of cover glasses with interdigital shaped ITO electrode were set face to face acting as top and bottom electrodes. Then the low concentration ANWF was placed between the two electrodes and Cu wires were attached to the electrodes by carbon paste. Finally, the electrodes were packaged by PDMS.

Supporting Information

Supporting Information is available from the Wiley Online Library or from the author.

[1] J. Yang, J. Chen, Y. Liu, W. Yang, Y. Su, Z. L. Wang, *ACS Nano* **2014**, *8*, 2649.
[2] F. R. Fan, J. Luo, W. Tang, C. Li, C. Zhang, Z. Tian, Z. L. Wang, *J. Mater. Chem. A* **2014**, *2*, 13219.
[3] K. Y. Lee, M. K. Gupta, S.W. Kim, *Nano Energy* **2015**, *14*, 139.
[4] L. Peng, L. Hu, X. Fang, *Adv. Funct. Mater.* **2014**, *24*, 2591.
[5] C. Chang, V. H. Tran, J. Wang, Y. K. Fuh, L. Lin, *Nano Lett.* **2010**, *10*, 726.
[6] K. Kim, S. H. Bae, C. T. Toh, H. Kim, J. H. Cho, D. Whang, T. W. Lee, B. Ozyilmaz, *ACS Appl. Mater. Interfaces* **2014**, *6*, 3299.
[7] Y. H. Ko, G. Nagaraju, S. H. Lee, J. S. Yu, *ACS Appl. Mater. Interfaces* **2014**, *6*, 6631.
[8] N. Cui, L. Gu, J. Liu, S. Bai, J. Qiu, J. Fu, X. Kou, H. Liu, Y. Qin, Z. L. Wang, *Nano Energy* **2015**, *15*, 321.
[9] Y. Qin, X. Wang, Z. L. Wang, *Nature* **2008**, *451*, 809.
[10] Y. Yang, J. H. Jung, B. K. Yun, F. Zhang, K. C. Pradel, W. Guo, Z. L. Wang, *Adv. Mater.* **2012**, *24*, 5357.
[11] L. Gu, N. Cui, L. Cheng, Q. Xu, S. Bai, M. Yuan, W. Wu, J. Liu, Y. Zhao, F. Ma, Y. Qin, Z. L. Wang, *Nano Lett.* **2013**, *13*, 91.
[12] W. Wu, L. Wang, Y. Li, F. Zhang, L. Lin, S. Niu, D. Chenet, X. Zhang, Y. Hao, T. F. Heinz, J. Hone, Z. L. Wang, *Nature* **2014**, *514*, 470.
[13] L. Lin, Y. Hu, C. Xu, Y. Zhang, R. Zhang, X. Wen, *Nano Energy* **2013**, *2*, 75.
[14] X.-S. Zhang, M.-D. Han, B. Meng, H.-X. Zhang, *Nano Energy* **2015**, *11*, 304.
[15] B. Meng, W. Tang, Z.-h. Too, X. Zhang, M. Han, W. Liu, H. Zhang, *Energy Environ. Sci.* **2013**, *6*, 3235.
[16] M. Han, X.-S. Zhang, B. Meng, W. Liu, W. Tang, X. Sun, W. Wang, H. Zhang, *ACS Nano* **2013**, *7*, 8554
[17] S.-H. Shin, Y.-H. Kim, M. H. Lee, J.-Y. Jung, J. Nah, *ACS Nano* **2014**, *8*, 2766.
[18] K. I. Park, M. Lee, Y. Liu, S. Moon, G. T. Hwang, G. Zhu, J. E. Kim, S. O. Kim, K. Kim do, Z. L. Wang, K. J. Lee, *Adv. Mater.* **2012**, *24*, 2999.
[19] B. Saravanakumar, S. Soyoon, S. J. Kim, *ACS Appl. Mater. Interfaces* **2014**, *6*, 13716.
[20] Y. Fujiyama, R. Tomokane, K. Tanaka, S. Akita, Y. Higashi, L. Pan, T. Nosaka, Y. Nakayama, *Jpn. J. Appl. Phys.* **2008**, *47*, 1991.
[21] H. Tang, Y. Lin, H. A. Sodano, *Adv. Energy Mater.* **2012**, *2*, 469.
[22] Y. Z. Long, M. Yu, B. Sun, C. Z. Gu, Z. Fan, *Chem. Soc. Rev.* **2012**, *41*, 4560.
[23] W.-S. Jung, Y.-H. Do, M.-G. Kang, C.-Y. Kang, *Curr. Appl. Phys.* **2013**, *13*, S131.
[24] X. Chen, S. Xu, N. Yao, Y. Shi, *Nano Lett.* **2010**, *10*, 2133.
[25] B. Im, H. Jun, K. H. Lee, S.-H. Lee, I. K. Yang, Y. H. Jeong, J. S. Lee, *Chem. Mater.* **2010**, *22*, 4806.
[26] S. J. Papadakis, Z. Gu, D. H. Gracias, *Appl. Phys. Lett.* **2006**, *88*, 233118.
[27] S. Shekhar, P. Stokes, S. I. Khondaker, *ACS Nano* **2011**, *5*, 1739.
[28] Y. Liu, J.-H. Chung, W. K. Liu, R. S. Ruoff, *J. Phys. Chem. B* **2006**, *110*, 14098.
[29] M. Zorn, M. N. Tahir, B. Bergmann, W. Tremel, C. Grigoriadis, G. Floudas, R. Zentel, *Macromol. Rapid Commun.* **2010**, *31*, 1101.

small
NANO MICRO

[30] Y. Huang, X. Duan, Q. Wei, C. M. Lieber, *Science* **2001**, *291*, 630.

[31] W. Wu, S. Bai, M. Yuan, Y. Qin, Z. L. Wang, T. Jing, *ACS Nano* **2012**, *6*, 6231.

[32] M. Manca, B. Cortese, I. Viola, A. S. Aricò, R. Cingolani, G. Gigli, *Langmuir* **2008**, *24*, 1833.

[33] A. D. Tserepi, M. E. Vlachopoulou, E. Gogolides, *Nanotechnology* **2006**, *17*, 3977.

[34] Y. H. Yan, M. B. Chan-Park, C. Y. Yue, *Langmuir* **2005**, *21*, 8905.

[35] Q. Tao, G. Y. Li, in *IEEE Conf. Nanotechnol.* PA, USA, December **2012**.

[36] S. J. Papadakis, J. A. Hoffmann, D. Deglau, A. Chen, P. Tyagi, D. H. Gracias, *Nanoscale* **2011**, *3*, 1059.

[37] D. A. van den Ende, B. F. Bory, W. A. Groen, S. van der Zwaag, *J. Appl. Phys.* **2010**, *107*, 024107.